

Gini-based Model Monitoring: A General Framework with an Application to Non-life Insurance Pricing

Alexej Brauer ¹ and Paul Menzel¹

¹ Actuarial Department, Allianz Versicherungs-AG, Königinstr. 28,
Munich, 80802, Bavaria, Germany.

Contributing authors: brauer.alexej@gmail.com; paul.menzel@tum.de;

Abstract

In a dynamic landscape where portfolios and environments evolve, maintaining the accuracy of pricing models is critical. To the best of our knowledge, this is the first study to systematically examine concept drift in non-life insurance pricing. We (i) provide an overview of the relevant literature and commonly used methodologies, clarify the distinction between virtual drift and concept drift, and explain their implications for long-run model performance; (ii) review and formalize common performance measures, including the Gini index and deviance loss, and articulate their interpretation; (iii) derive the asymptotic distribution of the Gini index, enabling valid inference and hypothesis testing; and (iv) present a standardized monitoring procedure that indicates when refitting is warranted. We illustrate the framework using a modified real-world portfolio with induced concept drift and discuss practical considerations and pitfalls.

Keywords: non-life insurance, concept drift, model monitoring, gini

Statements and Declarations:

Competing Interests: The authors have no conflicts of interest to declare that are relevant to the content of this article.

¹Author Contribution: A. Brauer led conceptualization, framework design, methodology, software implementation, investigation, most visualizations, and manuscript drafting, and contributed to the formal asymptotic analysis; P. Menzel led the formal asymptotic analysis and contributed to software, methodology, one visualization, and manuscript revision; both authors performed validation, critical review, and approved the final manuscript.

1 Introduction

In non-life insurance pricing, common tasks include predicting claim frequency, estimating claim severity, and modeling binary demand outcomes such as conversion prediction. Maintaining the accuracy of those models over time is a critical challenge in a dynamic landscape of evolving portfolios and market conditions. In this context, two key terms are often encountered: *model monitoring* and *model comparison*. These two terms are frequently used in the actuarial context of developing pricing models. The term *model monitoring*, also referred to as *backtesting*, pertains to testing a single model on at least two different datasets. This can occur either during the development phase, using training and validation/holdout data, or during the monitoring phase, using holdout data from the model update period versus new data from the current period. In contrast, *model comparison* is the process of comparing two different models on the same dataset to determine which one performs better. A schematic representation of both terms is given in Fig. 1.

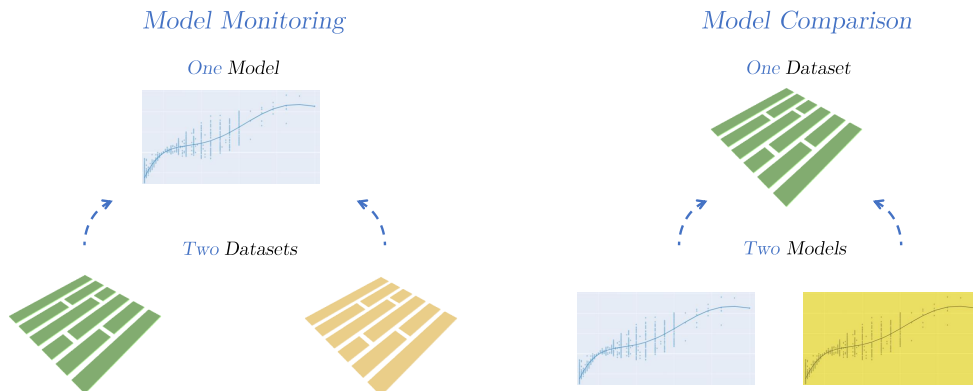


Fig. 1: Schematic representation of the Model Monitoring (left) and Model Comparison Framework (right). To visually distinguish datasets, the Apache Parquet logo color has been modified from its original design. The Apache Parquet logo is a trademark of the Apache Software Foundation.

In this work, we focus on *model monitoring*, which is often underemphasized in the actuarial literature yet is crucial for updating and maintaining pricing models over time. To the best of our knowledge, this is the first study to explicitly examine data drift in insurance pricing models; accordingly, we provide an overview of the relevant literature and a monitoring framework tailored to actuarial pricing practice. In contrast, *model comparison* is a more static process, typically performed during development to select the best model from a set of candidates (e.g., different covariates, hyperparameters, or algorithms).

However, when many models are in use, maintaining them can be very time-consuming and costly. And more importantly, a complete refitting of a pricing model often leads to changes in the feature contributions of the different risk factors due to the inherent correlation between the covariates in the training data and in smaller models due to statistical noise. This can lead to significant changes in the pricing of individual policies, particularly for segments that are not well-represented in the training data. Such changes are often undesirable

from a business perspective, as they can lead to unstable pricing and dissatisfaction among customers.

For this reason, model updates are often performed on a fixed time schedule, such as every one or two years, rather than being based on performance metrics. This, however, can lead to unnecessary updates and a suboptimal cost-benefit ratio in the model update process, as time might have been better spent on updating another model. Moreover, performing updates on a fixed time schedule can result in slow adaptation to changing market environments.

Therefore, this work concentrates on the *model monitoring* aspect. We establish the theoretical foundations for key evaluation metrics, notably deriving an asymptotic distribution for the sample Gini index. Based on this, we introduce a framework for assessing and monitoring the temporal robustness of non-life insurance pricing models to guide decisions on model refitting. For practical applicability, we present an illustrative example based on a modified real-world dataset in which we inject controlled levels of concept drift and discuss practical considerations and common pitfalls for real-world implementation.

1.1 Organization of this manuscript

In Sect. 2, we outline the theoretical background, review the relevant literature, and discuss *virtual drift* and *real concept drift* (see Sect. 2.1). Sect. 2.2 develops the theoretical foundations, covering auto-calibration, evaluation metrics and their properties, and derives the asymptotic distribution of the sample Gini index. Sect. 3 introduces a hypothesis-testing framework for monitoring models over time, detailed in Sect. 3.1. Sect. 3.2 illustrates the framework using a modified real-world insurance dataset, and Sect. 3.3 discusses practical considerations and common pitfalls. Finally, Sect. 4 concludes with a discussion and an outlook on future work.

2 Theoretical Background and Related Work

This section establishes the foundational concepts, definitions, and notation used throughout the paper. Unless specified otherwise: We assume a sufficiently rich probability space $(\Omega, \mathcal{A}, \mathbb{P})$ that supports all objects used in this manuscript. Random variables on this space are denoted by uppercase letters, e.g., X , with their realizations in lowercase, e.g., x . As a convention, we use bold uppercase letters to represent random vectors and lowercase bold letters for their realizations. For instance, we denote a random vector by $\mathbf{X} = (X_1, X_2, \dots, X_m)^\top$, and its realization by $\mathbf{x} = (x_1, x_2, \dots, x_m)^\top$, where $m \in \mathbb{N}$. We denote the cumulative distribution function (cdf) for a real-valued random vector \mathbf{X} , by $F_{\mathbf{X}}$.

As is common in regression modelling, we consider a random pair (Y, \mathbf{X}) on the probability space introduced above, where Y is a non-negative real-valued response with finite mean and \mathbf{X} denotes the covariate vector. Following the notation in Wüthrich (2023), we denote the family of potential distributions of (Y, \mathbf{X}) as \mathcal{F} , the conditional cdf of Y given \mathbf{X} as $F_{Y|\mathbf{X}}$ and the conditional mean functional T as

$$F_{Y|\mathbf{X}} \mapsto T(F_{Y|\mathbf{X}}) = \mathbb{E}[Y|\mathbf{X}] =: \mu^\dagger(\mathbf{X}). \quad (1)$$

The main goal in supervised learning is to estimate this true regression function $\mu^\dagger(\cdot)$ from a given dataset D of realizations. We denote this estimator by $\hat{\mu}(\cdot)$.

We consider here the following notation for datasets $D = \{(y_i, \mathbf{x}_i, v_i)\}_{i=1}^n$, comprising n observations. For each observation i , y_i is the response variable, \mathbf{x}_i is a k -dimensional vector

of covariates, and $v_i > 0$ represents the exposure. The elements in the covariate vector \mathbf{x}_i can be either numerical or categorical. Throughout this paper, we use $i \in \{1, \dots, n\}$ to index observations and $j \in \{1, \dots, k\}$ to index covariates, unless specified otherwise.

2.1 Virtual-Drift and Concept-Drift

The usual assumption in statistics is that we draw our data from i.i.d. random tuples (Y_i, \mathbf{X}_i) , $i \in \{1, \dots, n\}$, having the same distribution as (Y, \mathbf{X}) . The common further assumption is that the data-generating process is stationary, i.e., that the distribution of (Y, \mathbf{X}) does not change over time. In non-life insurance modeling, one often trains a model on data from a given period (e.g., years 2020-2023) and assumes this data is under global trend assumptions representative of a later period (e.g., 2025), when the model will be used in production. However, while this assumption is typically reasonable when comparing training and holdout datasets drawn from the same period, it is frequently violated in production datasets due to changes in the underlying population, customer behavior, the data-collection process, and — last but not least — the real-world environment.

Related Work History: Detecting changes in the underlying data-generating process has been studied extensively for decades (see, e.g., Schlimmer and Granger (1986); Widmer and Kubat (1996)) and remains an active area of research. Although work evolves in parallel across several communities, a key consolidation is provided by the survey articles Gama et al (2014) and Lu et al (2019), which systematize methods, clarify definitions (e.g., *virtual* vs. *real concept drift*), and summarize the state of the art up to 2014 and 2019, respectively. We adopt their terminology in what follows.

More recent advances and surveys include: for scenarios where data labeling is challenging, see, e.g., Ackerman et al (2021); for neural networks, see, e.g., the survey Rabanser et al (2019); for data drift detection in large-scale systems, see Mallick et al (2022); and more recently for drift detection using deep neural networks and autoencoders, see Hu et al (2025). For a formulation of drift as a distribution process and a survey of the literature on unsupervised drift detection, the authors refer to Hinder et al (2024).

Terminology: Because the terminology is more prevalent in the machine learning community—for example, in online learning of classification tasks, and process mining—and less so in actuarial science, we provide a brief overview of the terminology in an actuarial context. As Gama et al (2014) describe in their survey, the literature uses many different terms to refer to changes in the data-generating process over time. Common expressions include *data drift*, *covariate shift*, *virtual shift*, *temporary drift*, *sampling shift*, *feature change*, *concept drift*, *conditional change* and *real concept drift*. We also note that terminology is not used consistently across the literature.

For consistency, we follow the definitions of Gama et al (2014) and distinguish two main types of drift: *virtual drift* and *real concept drift*. Here, *virtual drift* refers to changes in the distribution of the features \mathbf{X} , i.e., $F_{\mathbf{X}}$, and, importantly, occurs without changing the conditional distribution $F_{Y|\mathbf{X}}$; thus the true regression function $\mu^\dagger(\mathbf{X})$ (1) remains unchanged. By contrast, *real concept drift* refers to changes in the conditional distribution $F_{Y|\mathbf{X}}$ and thus in the true regression function $\mu^\dagger(\mathbf{X})$. Notably, this change in the conditional distribution can occur with or without a change in $F_{\mathbf{X}}$. Table 1 summarizes the definitions and common alternative names for *virtual drift* and *real concept drift* used in the literature.

Furthermore, we refer to changes in the distribution of the features $F_{\mathbf{X}}$ as *covariate drift*; note that this can result in either *virtual drift* or *real concept drift*.

Table 1: *virtual drift* and the *real concept drift*:

	<i>virtual drift</i>	<i>real concept drift</i>
Definition	Changes in $F_{\mathbf{X}}$ without changing $F_{Y \mathbf{X}}$	Changes in $F_{Y \mathbf{X}}$
Also called in literature sometimes	data drift, virtual shift, temporary drift, sampling shift, feature change covariate shift	data drift, conditional change, concept drift,

The authors acknowledge that detecting *virtual drift* is very important in the insurance industry for understanding how the portfolio evolves over time. However, our interest lies in changes in predictive performance over time and in identifying when a model should be updated; accordingly, we restrict attention to *real concept drift* rather than *virtual drift*. The phenomenon in which the predictive performance of a deployed model degrades over time is often referred to in the literature as *model drift*.

While we now establish the different drift terms, it is important to note, that even if only a *virtual drift* occurs (i.e., no change in the true regression function $\mu^\dagger(\mathbf{X})$), there can still be an actual change in the performance of the estimator of the regression function (i.e., the model $\hat{\mu}(\mathbf{X})$). This is because the model $\hat{\mu}(\mathbf{X})$ may not be trained on a sufficiently rich data set and thus may not generalize well. If the exposure of new data increases in regions where the model performs poorly, its performance will degrade. While insufficient data coverage is an important issue, in the following theoretical section we focus on *real concept drift* and therefore assume that the model is trained on a sufficiently large data set.

Real Concept Drift Types: There are typically 4 types of reasons distinguished for *real concept drift* discussed in the literature. These are *sudden or abrupt drift*, *gradual drift*, *incremental drift*, and *recurrent drift* (see Lu et al (2019) for a comprehensive overview and visualization). In this manuscript, we focus on the first three types of drift.

Concept Drift Detection Method Types: There are several methods for detecting *real concept drift* that can be broadly categorized into the following four main families. These are:

- **Data Distribution-based Methods:** Typical examples of such methods involve computing distribution distance measures such as Kolmogorov-Smirnov, Wasserstein metric, Kullback-Leibler divergence and Jensen-Shannon metric between the old data and the new data. See, for example, Section 4.3 of Hinder et al (2024).
- **Dimensionality Reduction-Based Methods:** Another common approach is to compare reconstruction errors obtained via PCA or autoencoders. Furthermore, domain classifier approaches are often used in this context, in which one trains a classifier to distinguish between old and new data. If the classifier performs well, it indicates a significant difference between the two distributions, suggesting the presence of *covariate drift*. See, for example, Rabanser et al (2019).
- **Error Rate-Based Methods:** These algorithms are typically used for classification tasks and are designed to monitor a predictive model’s performance across time windows. When a statistically significant change in the error rate is detected, a drift alarm is triggered. Very influential examples include the Drift Detection Method (DDM) Gama et al (2004), the

Statistical Test of Equal Proportions (STEPD) [Nishida and Yamauchi \(2007\)](#), and the Adaptive Windowing (ADWIN) [Bifet and Gavaldà \(2007\)](#).

- Multiple Hypothesis Methods: These drift detection methods combine multiple different algorithms either in parallel or in a hierarchical manner to detect drift. See, for example, Section 3.2.3 in [Lu et al \(2019\)](#).

The approach in this manuscript follows the tradition of the error rate-based methods DDM and STEPDP but adapts it from classification to regression in insurance: instead of traditional classification error measures, we monitor the Gini index for non-classification tasks and derive its asymptotic properties to enable statistical tests.

2.2 Auto-Calibration, Metrics and their Properties

Since auto-calibration is a crucial requirement for our monitoring framework and the upcoming asymptotic proof, we first define it in Section 2.2.1. Furthermore, given its popularity in the actuarial literature, we briefly describe the deviance loss and highlight its key limitations for model monitoring. We then introduce the Gini index in Section 2.2.3, on which we build our monitoring framework.

2.2.1 Auto-Calibration

We require the auto-calibration property for our monitoring framework. Like described in [Krüger and Ziegel \(2021\)](#) and [Wüthrich and Merz \(2023\)](#), we define it as follows:

Definition 1 (Auto-Calibration). A random variable Z is an auto-calibrated forecast of a random variable Y if

$$\mathbb{E}[Y | Z] = Z \quad \text{a.s.}$$

Furthermore, a regression function $\hat{\mu}(\cdot)$ is called auto-calibrated for Y if

$$\hat{\mu}(\mathbf{X}) = \mathbb{E}[Y | \hat{\mu}(\mathbf{X})] \quad \text{a.s.} \tag{2}$$

In insurance pricing, auto-calibration is a valuable property of a regression function, as pointed out by [Wüthrich \(2023\)](#), because it ensures that each price cohort $\hat{\mu}(\mathbf{X})$ is, on average, self-financing; that is, $\hat{\mu}(\mathbf{X})$ covers the cohort's expected claims, thus avoiding cross-financing. Another valuable implication of auto-calibration is that it ensures the regression function $\hat{\mu}(\cdot)$ is unbiased at the portfolio level, which is a minimal requirement for insurance pricing.

It follows from the definition of $\mu^\dagger(\cdot)$ (see 1) and the tower rule, the true regression function $\mu^\dagger(\mathbf{X}) = \mathbb{E}[Y | \mathbf{X}]$ is an auto-calibrated forecast of Y .

Furthermore, it is important to emphasize that, in general, neither modern machine learning methods nor the industry-standard GLMs are auto-calibrated or unbiased at the portfolio level.

However, when using the canonical link function, we can ensure unbiasedness at the portfolio level for GLMs (see e.g. Proposition 4.1 in [Charpentier \(2024\)](#)).

To assess auto-calibration in practice, one may test whether the empirical concentration and Lorenz curves coincide, which (for unbiased estimators) is equivalent to testing auto-calibration (see Section 4 of [Denuit et al \(2024\)](#)). In the case of a discrete, finite regression function, one can also apply one of the three test statistics with known asymptotic distributions under auto-calibration proposed by [Wüthrich \(2025\)](#). These procedures detect systematic deviations of predictions from observed outcomes across different segments of the data.

To improve the model’s calibration, one can apply a transformation to the model prediction. By doing so, we define the balance-corrected version of the prediction $\hat{\mu}_{BC}(\cdot)$ as $\hat{\mu}_{BC}(\mathbf{X}) = \mathbb{E}[Y|\hat{\mu}(\mathbf{X})]$ (see Section 5.1 in [Denuit et al \(2021\)](#) and Remarks 7.18 in [Wüthrich and Merz \(2023\)](#)). This transformation helps restore the auto-calibration property, ensuring that the estimator remains reliable and accurate across varying data conditions.

2.2.2 Deviance loss

Given the popularity of generalized linear models (GLMs) [Nelder and Wedderburn \(1972\)](#) in the insurance industry, the deviance loss is widely used as a loss measure in the non-life insurance literature for *model comparison*. This also holds beyond the GLM framework; see, e.g., [Wüthrich and Merz \(2023\)](#); [Richman and Wüthrich \(2023\)](#); [Brauer \(2024\)](#); [Holvoet et al \(2025\)](#); [Richman et al \(2025\)](#).

Since these terms are sometimes confused, we briefly clarify the difference between the deviance and the deviance loss. The deviance is usually defined in the GLM framework as the following difference between two log-likelihoods.

Definition 2 (Deviance). The deviance is then defined as the following difference between the log-likelihoods:

$$\bar{D}(y, \hat{y}) = 2\varphi[\ell(\hat{\beta}_{\max}) - \ell(\hat{\beta})].$$

Where φ is the dispersion parameter and $\ell(\cdot)$ denotes the log-likelihood of the chosen GLM family. Here $\ell(\hat{\beta}_{\max})$ denotes the log-likelihood of the saturated model, and $\ell(\hat{\beta})$ denotes the log-likelihood of the model of interest.

The deviance loss, in turn, can be defined as a scaled version of the deviance:

Definition 3 (Deviance loss).

$$D(y, \hat{y}) = \frac{1}{n\varphi}\bar{D}(y, \hat{y}),$$

where n is the number of observations.

Typically, the deviance loss is preferred for *model comparison* over the deviance because the latter scales with the number of observations. Another way to express the deviance loss is as a weighted sum of unit deviances (see Equations (4.8) and (4.9) in [Wüthrich and Merz \(2023\)](#)).

$$D(y, \hat{y}) = \frac{1}{n} \sum_{i=1}^n \frac{v_i}{\varphi} d(y_i, \hat{y}_i) \tag{3}$$

Here, the unit deviance can be interpreted as a statistic that quantifies the discrepancy between the prediction \hat{y}_i and the actual observation y_i . See Chapter 4 in [Wüthrich and Merz \(2023\)](#) for more details and examples regarding the different underlying distributions.

The deviance loss is an important statistic for GLMs because maximizing the likelihood function corresponds to minimizing the deviance loss (see Corollary 4.5 in [Wüthrich and Merz \(2023\)](#)). Moreover, it is a strictly consistent scoring function that measures how well the model fits the data relative to the saturated model.

However, although very useful for *model comparison*, the deviance loss has several disadvantages when used for *model monitoring*:

- First, it is sensitive to outliers, which can trigger false alarms when tracking model performance over time.
- Second, it lacks an absolute scale; its magnitude is not directly interpretable across datasets.

- Third, it is, in practice, highly sensitive to differences in the data preparation process between datasets. While this is usually not limiting for *model comparison*, where the same dataset and data preparation are used for all models, it is undesirable for *model monitoring*. See also Pitfall B in Section 3.3 for a commonly underestimated change in the deviance due to data preparation.

For this reason, we instead advocate the Gini index as the primary metric in the following monitoring framework.

2.2.3 Gini Index

The Gini index is a rank-based metric that quantifies how well a model discriminates between different outcomes. It is popular in the machine learning community for *model comparison*. In the actuarial community, however, it is less widely used, partly because it is, in general, not a strictly consistent scoring function; optimizing it (i.e., maximizing it) does not necessarily lead to the best model in regards to the true regression function $\mu^\dagger(\mathbf{X})$. Our decision to use the Gini index as a monitoring measure is inspired by the results of Denuit et al (2024) and Wüthrich (2023), where the former provides a framework for detecting auto-calibration and the latter shows that the Gini index is a strictly consistent scoring function within the class of auto-calibrated regression models. We follow the notation and definitions of Wüthrich (2023).

Before defining the Gini index, we note that there is not only one definition in the literature. For example, in Denuit et al (2024) the Gini index is defined purely via the Lorenz curve, which depends only on the predictions and not on the response variable Y . This definition is popular and widely used in economics. In Holvoet et al (2025), a version of the Gini index is provided to compare tariff structures between two models by evaluating their respective Lorenz curves. However, in the machine learning community, the Gini index is commonly defined via the Cumulative Accuracy Profile (CAP) curve. The CAP curve depends on both the predictions $\hat{\mu}(\mathbf{X})$ and the response variable Y . We use the latter definition in this manuscript. An overview of the different definitions and their relationships under autocalibration is given in Wüthrich (2023).

We begin by introducing the CAP.

Definition 4 (Cumulative accuracy profile). Let $\alpha \in (0, 1)$. The CAP is defined as:

$$\text{CAP}_{Y, \hat{\mu}(\mathbf{X})}(\alpha) := \frac{1}{\mathbb{E}[Y]} \mathbb{E} \left[Y \mathbb{1}_{\{\hat{\mu}(\mathbf{X}) > F_{\hat{\mu}(\mathbf{X})}^{-1}(1-\alpha)\}} \right] \in [0, 1]. \quad (4)$$

Where $\hat{\mu}(\mathbf{X})$ is assumed to have a continuous distribution function $F_{\hat{\mu}(\mathbf{X})}$ for all $(Y, \mathbf{X}) \sim F \in \mathcal{F}$. Furthermore, $F_{\hat{\mu}(\mathbf{X})}^{-1}$ denotes the left-continuous inverse of $F_{\hat{\mu}(\mathbf{X})}$.

Note that the concentration curve CC, which is more popular in the insurance community (see Definition 3.1 in Denuit et al (2019)), is related to the CAP via $\text{CAP}_{Y, \hat{\mu}(\mathbf{X})}(\alpha) = 1 - \text{CC}_{Y, \hat{\mu}(\mathbf{X})}(1 - \alpha)$.

Definition 5 (Gini index). Using the CAP, the Gini index $G_{Y, \hat{\mu}(\mathbf{X})}$ is defined for $\hat{\mu}(\mathbf{X})$ and Y , assuming they have continuous distribution functions $F_{\hat{\mu}(\mathbf{X})}$ and F_Y , respectively, as:

$$G_{Y, \hat{\mu}(\mathbf{X})} := \frac{\int_0^1 \text{CAP}_{Y, \hat{\mu}(\mathbf{X})}(\alpha) d\alpha - \frac{1}{2}}{\int_0^1 \text{CAP}_{Y, Y}(\alpha) d\alpha - \frac{1}{2}}. \quad (5)$$

Analogously to Wüthrich (2023), we provide a geometric visualization of the two CAP curves and the areas corresponding to the integrals in Figure 2 and Equation (6).

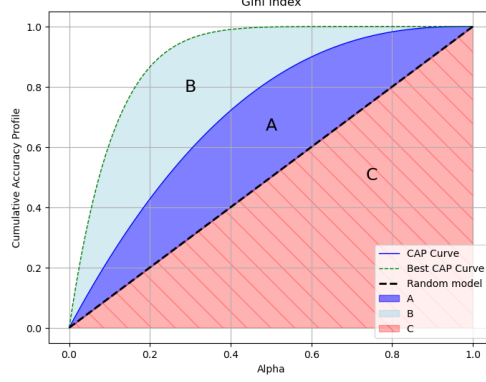


Fig. 2: Geometric visualization of the Gini index.

In Figure 2 the curve $\text{CAP}_{Y, \hat{\mu}(\mathbf{X})}(\alpha)$ is referred to as the CAP curve, and $\text{CAP}_{Y, Y}(\alpha)$ is referred to as the Best CAP curve, for all $\alpha \in (0, 1)$. The integral from 0 to 1 of $\text{CAP}_{Y, \hat{\mu}(\mathbf{X})}(\alpha)$ equals the area under the CAP curve, i.e. the sum of areas $A + C$. Similarly, the integral from 0 to 1 of $\text{CAP}_{Y, Y}(\alpha)$ equals the area under the Best CAP curve, i.e. the sum of areas $A + B + C$. Using these interpretations and the fact that area $C = \frac{1}{2}$, we obtain the geometric interpretation of the Gini index:

$$G_{Y, \hat{\mu}(\mathbf{X})} = \frac{\int_0^1 \text{CAP}_{Y, \hat{\mu}(\mathbf{X})}(\alpha) d\alpha - \frac{1}{2}}{\int_0^1 \text{CAP}_{Y, Y}(\alpha) d\alpha - \frac{1}{2}} = \frac{A + C - C}{A + B + C - C} = \frac{A}{A + B}. \quad (6)$$

Asymptotic Normality of the Gini Index: Because the Gini index will be used in our monitoring framework, it is of practical importance to understand its distribution. An asymptotic normality result for the economic Gini index is provided by Section 3 in Davidson (2009). This inspired us to prove the asymptotic normality of the machine learning Gini defined in Definition 5. We first state the theorem and then provide the proof.

Theorem 1 (Asymptotic Normality of the Gini Index). *Assume $(Y_i, \mathbf{X}_i) \sim F \in \mathcal{F}$ i.i.d. and let $\hat{\mu}(\cdot)$ be an auto-calibrated estimator. Suppose $\mathbb{E}[Y] < \infty$ and $\mathbb{E}[\hat{\mu}(\mathbf{X})] < \infty$. Further assume that Y and $\hat{\mu}(\mathbf{X})$ have continuous distribution functions F_Y and $F_{\hat{\mu}(\mathbf{X})}$, respectively. Let the combined distribution function of $(Y, \hat{\mu}(\mathbf{X}))$ be denoted by $F_{Y, \hat{\mu}(\mathbf{X})}$ and the Gini index $G_{Y, \hat{\mu}(\mathbf{X})}$ be defined as in Definition 5.*

Then there is a functional T such that the Gini index can be written as $T(F_{Y, \hat{\mu}(\mathbf{X})}) = G_{Y, \hat{\mu}(\mathbf{X})}$ and the plug in estimator $\hat{G}_{Y, \hat{\mu}(\mathbf{X})} := T(\hat{F}_{Y, \hat{\mu}(\mathbf{X})})$ for the Gini index is asymptotically normal distributed. Specifically it holds for some $\sigma^2 > 0$, that

$$\sqrt{n}(\hat{G}_{Y, \hat{\mu}(\mathbf{X})} - G_{Y, \hat{\mu}(\mathbf{X})}) \xrightarrow{d} N(0, \sigma^2).$$

We provide here a sketch of the proof; full details are given in the Appendix.

Proof sketch. First represent the Gini index as a statistical functional T . Then show that T is Hadamard differentiable at $F_{Y, \hat{\mu}(\mathbf{X})}$. And finally, combine the empirical-process convergence $\sqrt{n}(\hat{F}_{Y, \hat{\mu}(\mathbf{X})} - F_{Y, \hat{\mu}(\mathbf{X})}) \rightsquigarrow \mathbb{G}_F$ with the functional Delta Method to obtain $\sqrt{n}(\hat{G}_{Y, \hat{\mu}(\mathbf{X})} - G_{Y, \hat{\mu}(\mathbf{X})}) \xrightarrow{d} N(0, \sigma^2)$. \square

For the full proof, see Appendix A.

Because the joint distribution $(Y, \mathbf{X}) \sim F \in \mathcal{F}$ is generally unknown in practice, we use empirical distribution functions to estimate the Gini index. The empirical CAP is defined as follows (see Equation (4.12) in Wuthrich et al (2025)):

Definition 6 (Empirical cumulative accuracy profile). By first ordering and relabeling the observation Y_i to $Y_{(i)}$ based on the order statistics of the predictions, $\hat{\mu}(\mathbf{X}_{(1)}) < \hat{\mu}(\mathbf{X}_{(2)}) < \dots < \hat{\mu}(\mathbf{X}_{(n)})$, the empirical CAP is defined as:

$$\widehat{\text{CAP}}_{Y, \hat{\mu}(\mathbf{X})}(\alpha) = \frac{1}{\sum_{i=1}^n Y_i} \sum_{i=\lceil(1-\alpha)n\rceil+1}^n Y_{(i)}.$$

Note that $\widehat{\text{CAP}}_{Y, \hat{\mu}(\mathbf{X})}(\alpha)$ depends on the predictions $\hat{\mu}(\mathbf{X})$ via the ordering, since each observation $Y_{(i)}$ corresponds to the i -th smallest predicted value $\hat{\mu}(\mathbf{X}_{(i)})$ among $\{\hat{\mu}(\mathbf{X}_l)\}_{l=1}^n$. Using Definition 6, we define the empirical version of the Gini index as:

Definition 7 (Empirical Gini index). The empirical Gini index is defined as follows.

$$\widehat{G}_{Y, \hat{\mu}(\mathbf{X})} = \frac{\int_0^1 \widehat{\text{CAP}}_{Y, \hat{\mu}(\mathbf{X})}(\alpha) d\alpha - \frac{1}{2}}{\int_0^1 \widehat{\text{CAP}}_{Y, Y}(\alpha) d\alpha - \frac{1}{2}}.$$

We note that we do not explicitly derive the asymptotic variance of the Gini index described in Theorem 1. However, because we show that the limiting distribution is normal and we assume that the observations from a fixed time point are i.i.d., we can assume that a bootstrap approach is *consistent* (see Section 4.3 in Wüthrich and Merz (2023)). Therefore, we estimate the parameters of the asymptotic normal distribution via the following bootstrap approach:

1. Step: Generate n predictions $\hat{\mu}(\mathbf{X}_i)$ for $i = 1, \dots, n$.
2. Step: Generate B bootstrap samples of size n by sampling with replacement from the set of tuples $\{(Y_i, \hat{\mu}(\mathbf{X}_i))\}_{i=1}^n$.
3. Step: For each bootstrap sample $b = 1, \dots, B$, calculate the empirical Gini index $\widehat{G}_{Y, \hat{\mu}(\mathbf{X})}^{(b)}$.
4. Step: Estimate the asymptotic mean and standard deviation of the Gini index on the provided dataset using the bootstrap samples.

Note that this is not similar to bootstrap estimation of the generalization error because we are not refitting the model on each bootstrap sample.

To provide a visual illustration of the (asymptotic) normality of the Gini index, we follow the steps above for a very popular dataset and model in non-life insurance literature which is described in Section 3.2.

We applied the bootstrap steps described above to the holdout of this dataset and the fitted GLM model. In Figure 3, we show histograms of the bootstrap Gini indices for varying numbers of bootstrap samples B (left) and varying holdout sample sizes n (right).

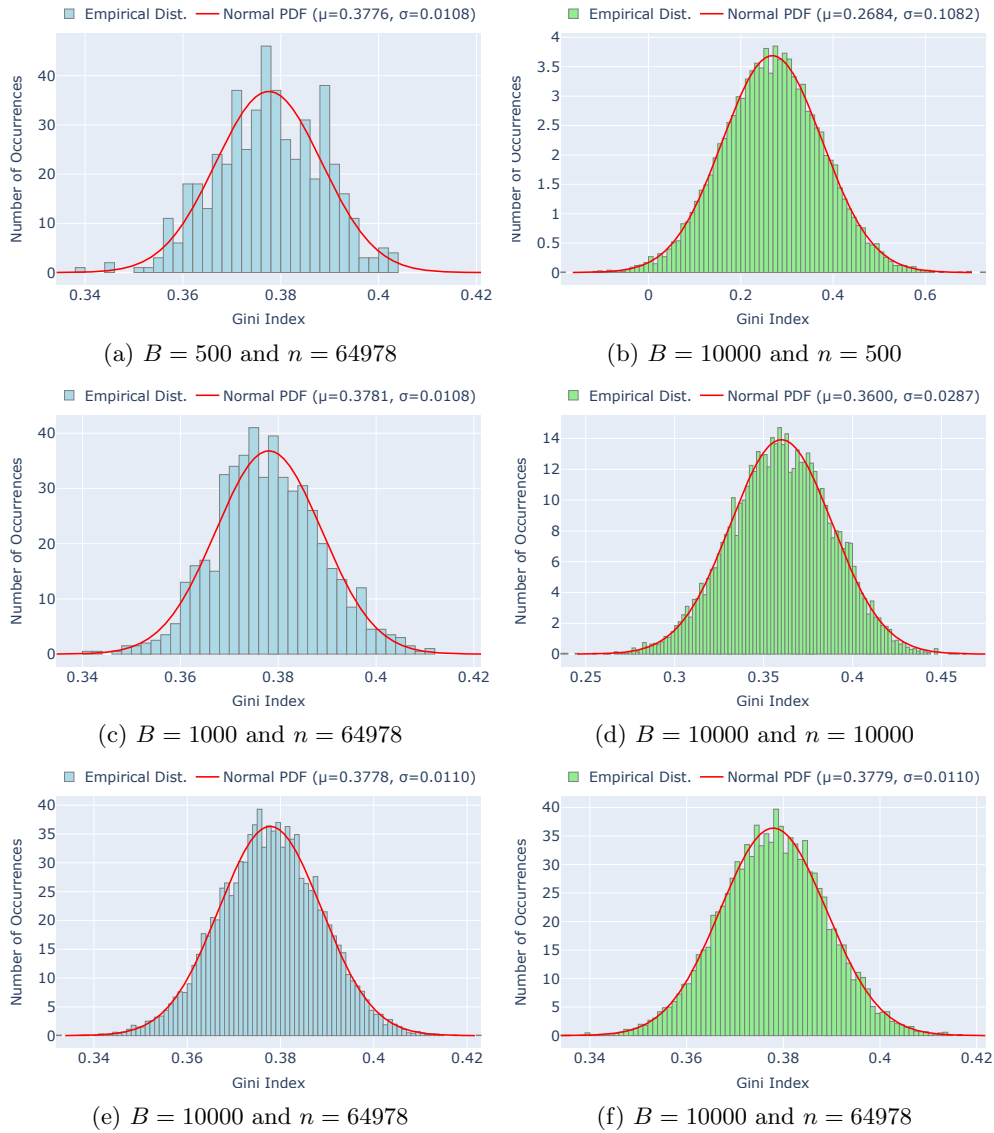


Fig. 3: Histograms of the bootstrap Gini indices for varying numbers of bootstrap samples B (left) and varying holdout sample sizes n (right).

As expected, the histograms approximate a normal distribution, and the approximation improves with larger bootstrap sample sizes B . Furthermore, the standard deviation decreases with larger holdout sample sizes n . This aligns with intuition for model monitoring frameworks: if the holdout sample size is small, the model was likely trained on a small dataset, and the model error (as measured by the Gini index) should also be more volatile.

Using the results established in this section, we outline a model monitoring framework in the next section.

3 Model monitoring framework and practical considerations

First, we will outline our general framework for model monitoring and then we will provide common pitfalls and practical considerations.

3.1 General Framework for Model Monitoring

On one hand, it is also important not to miss a necessary update of a model in order to maintain the model’s performance. But on the other hand, as noted in the introduction, the model update process is time-consuming, complex, and may introduce instability into the pricing model; therefore, changes should not be made lightly. This, in turn, prompts the question of whether an update is needed.

We first outline the model update process to clarify which information is available at the decision point. We do this by providing an example of an annual model update process with a fixed window size, though the same logic applies to other update frequencies. In a typical annual cycle, the incumbent model is either recalibrated with new data or replaced by a newly developed model that incorporates the latest data. Because models are trained on prior-year data while data from the update year is not yet fully observed or validated, a lag arises. This lag is further increased by the time required for model development, validation and governance. Therefore, in an annual cycle, a one-year lag can arise. Consequently, the most recent data used to train or assess the model comes from the year preceding the update. In Figure 4, an example timeline of a model update cycle in 2024 is shown. In this example,

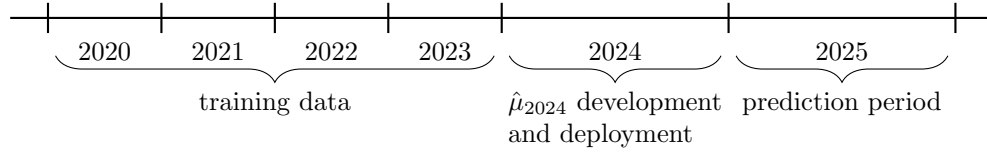


Fig. 4: Example timeline of a model update cycle in 2024. The index 2024 in $\hat{\mu}_{2024}$ indicates the year in which the model is developed.

claim data from 2020–2023 is used to train a model. The model $\hat{\mu}_{2024}(\cdot)$ is then developed in 2024 without using any 2024 data for training or validation. This model is subsequently deployed to predict, e.g., claim counts for 2025.

The question we seek to answer in the 2025 update cycle is whether the model created in 2024 $\hat{\mu}_{2024}$ using data from 2020–2023 can be reused (with minor recalibration) and deployed in 2025 to produce predictions for 2026, or whether a new model, $\hat{\mu}_{2025}$, should be developed. An illustration of this timeline is shown in Figure 5. This decision should be made in 2025, when data for 2024 becomes available. To guide this decision, we first compute, following Section 2.2.3, the mean $\hat{\mathbb{E}} \left[G_{Y, \hat{\mu}_{2024}}^{old-data}(\mathbf{x}) \right]$ and standard deviation $\hat{\sigma} \left[G_{Y, \hat{\mu}_{2024}}^{old-data}(\mathbf{x}) \right]$ of the Gini index on the training-period holdout dataset. We then compute the Gini index on

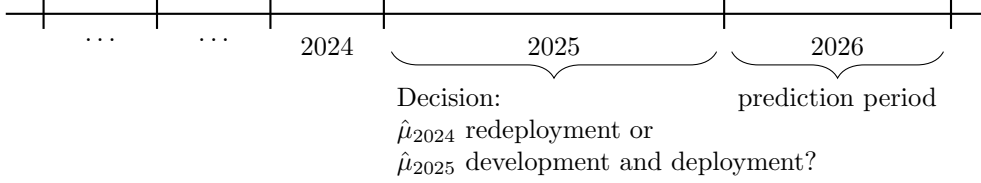


Fig. 5: Example timeline for decision-making in 2025. The index 2024 in $\hat{\mu}_{2024}$ indicates the year in which the model is developed.

a similarly sized dataset from 2024 $\hat{G}_{Y, \hat{\mu}_{2024}(\mathbf{X})}^{new-data}$. We can then apply the following hypothesis test. Under the assumption of no *real concept drift*, the Gini index on the new data should come from the same distribution as the holdout Gini values from the training period, i.e., under the null hypothesis H_0 .

Null hypothesis:

$$H_0 : \hat{G}_{Y, \hat{\mu}_{2024}(\mathbf{X})}^{new-data} \sim \mathcal{N} \left(\hat{\mathbb{E}} \left[G_{Y, \hat{\mu}_{2024}(\mathbf{X})}^{old-data} \right], \hat{\sigma} \left[G_{Y, \hat{\mu}_{2024}(\mathbf{X})}^{old-data} \right]^2 \right).$$

Test statistic:

$$z = \frac{\hat{G}_{Y, \hat{\mu}_{2024}(\mathbf{X})}^{new-data} - \hat{\mathbb{E}} \left[G_{Y, \hat{\mu}_{2024}(\mathbf{X})}^{old-data} \right]}{\hat{\sigma} \left[G_{Y, \hat{\mu}_{2024}(\mathbf{X})}^{old-data} \right]}.$$

p-value (two-sided):

$$p = 2(1 - \Phi(|z|)),$$

where $\Phi(\cdot)$ is the standard normal CDF. We decide at level α to reject H_0 if $p < \alpha$ (equivalently, if $|z| > \Phi^{-1}(1 - \frac{\alpha}{2})$); otherwise, we fail to reject H_0 . Regarding interpretation, the test statistic z measures changes in Gini performance in standard-deviation units; negative values ($z < 0$) indicate deterioration and positive values indicate improvement. For example, a z -value of -1 (corresponding to a p-value of ≈ 0.32) means that the Gini performance on the new data is one standard deviation worse than the average Gini performance in the training period. A z -value of -1.96 (corresponding to a p-value of ≈ 0.05) means that the Gini performance on the new data is nearly two standard deviations worse than the average Gini performance in the holdout of the training period.

Note that this is a two-sided test, as we want to detect both deterioration and improvement in model performance, one can also use a one-sided test if only deterioration is of interest.

In the next section, we present a simple illustrative example; subsequently, we discuss practical considerations.

3.2 Illustration example

To provide a simple illustrative example of the above-mentioned monitoring framework, we use a very popular dataset and model in non-life insurance. Just as MNIST is the de facto “hello world” dataset in computer vision (see, e.g., [Ackerman et al \(2021\)](#)), the FreMTPL2freq [Dutang and Charpentier \(2018\)](#) dataset becomes the de facto “hello world” dataset for non-life insurance pricing. It is a well-known French motor third-party liability (MTPL) claim-frequency dataset that is widely used in the actuarial literature for benchmarking and interpreting new methods (see, e.g., [Lorentzen and Mayer \(2020\)](#), [Richman](#)

and Wüthrich (2023), Wüthrich and Merz (2023), Brauer (2024), Holvoet et al (2025)). We use version 1.0–8 of the dataset, as in the cited literature.

Since the dataset is already well documented in the literature, we briefly summarize where the data exploration, preprocessing, and model-fitting steps can be found. For data exploration, we refer to the tutorial by Noll et al. Noll et al (2020). Furthermore, we use the same data-cleaning process described in Appendix B of Wüthrich and Merz (2023). For data preparation, we follow the same feature engineering as in Section 5.3.4 of Wüthrich and Merz (2023). For the train/test split, we apply the same split used by most manuscripts that use this dataset, as described in Listing 5.2 of Wüthrich and Merz (2023). The test set contains 67,801 observations, whereas the training set contains 610,206.

We fit the same Poisson GLM with a log link as GLM3 in Section 5.3.4 of Wüthrich and Merz (2023) on the training dataset. The unpenalized GLM is fitted with the scikit-learn API Buitinck et al (2013) using the Newton–Cholesky solver. We verified that this GLM matches the one reported in the literature by computing the Poisson deviance on the holdout dataset and comparing it to the published value.

Finally, to ensure that systematic time-splitting is not an issue in the upcoming analysis (see Pitfall B in Section 3.3), we pre-aggregate the holdout dataset. We do this as a precaution because it is unclear whether the column “IDpol” is a true policyholder identifier or a time-period-policyholder identifier created by the data provider. We pre-aggregate at the level of unique covariate combinations (i.e., across all covariates used in the model) so that each covariate combination appears only once, along with its total exposure, total claim count, and corresponding exposure-weighted prediction. After this aggregation, the observation count of the holdout dataset decreases only slightly to 64,978.

The above-mentioned GLM3 depends on several covariates, including the driver’s age (`DriveAge` in the dataset), which we use to simulate concept drift. To illustrate the monitoring framework, we create a new dataset by augmenting the holdout dataset and simulating concept drift. We do this by artificially redistributing a fixed number of claims across different age groups while keeping the total claim count constant. Specifically, we transfer 100 claims in Scenario 1, 150 claims in Scenario 2, and 200 claims in Scenario 3 (approximately 3.8%, 5.7%, and 7.56% of all claims in the holdout dataset, respectively) from drivers aged 25–35 years to drivers aged 35–45 years.

This simulation mimics a setting in which claim frequencies shift between demographic groups over time, for example due to changing driving behaviors within specific age cohorts. For the claim reduction, we randomly sample policyholders in the younger age group with at least one claim and reduce their claim count by one. For the claim increase, we randomly sample policyholders in the older age group (regardless of their original claim count) and increase their claim count by one.

This redistribution creates a detectable shift in the age-specific claim frequency pattern while maintaining the overall portfolio claim count, allowing us to assess the sensitivity of our monitoring framework to localized distributional changes. Figure 6 visualizes the changes introduced by this procedure.

In each plot, bars represent exposure, the blue line shows predicted claim frequency, and the green line shows observed claim frequency. Subfigure (a) shows the original claim frequency by age; (b)–(d) show progressively more severe claim redistributions from the driver age group (25–35) to (35–45) years for Scenarios 1–3.

By construction, the overall observed claim frequency is unchanged. However, the observed age-specific claim frequencies do change due to the redistribution. In contrast, the model’s

predicted claim frequency remains unchanged—both overall and by age group, because policyholder features do not change.

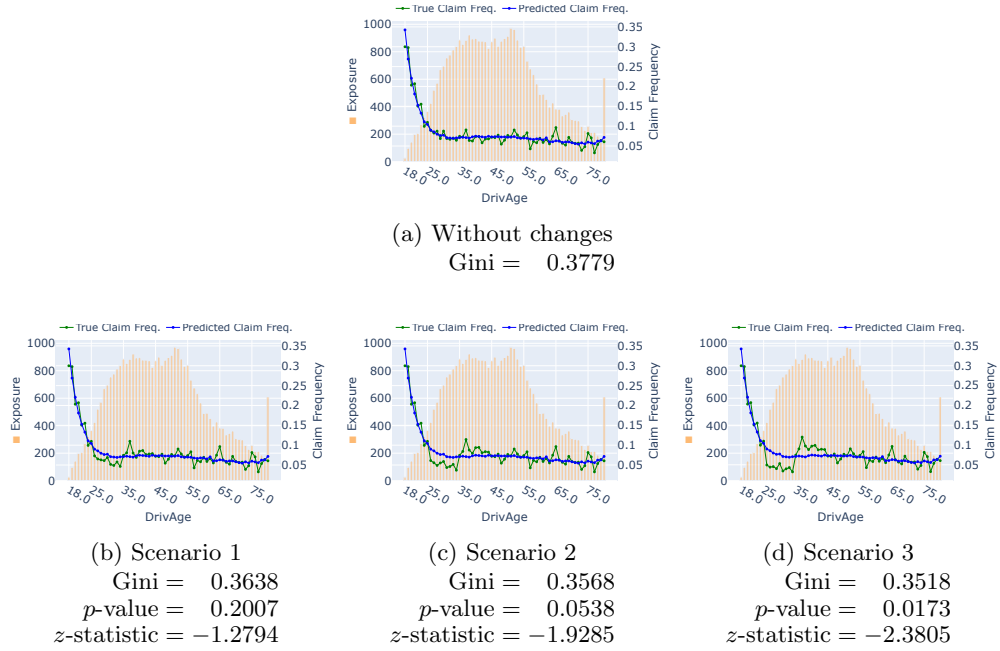


Fig. 6: Illustrative example showing the effect of induced concept drift by redistributing claims between age groups.

We apply the framework introduced in Section 3.1 by calculating the Gini index on both the original holdout dataset and the modified datasets from Scenario 1 and Scenario 2. Using the bootstrap procedure described in Section 2.2.3, we estimate the parameters of the null distribution ($\sigma = 0.0109$) and subsequently compute the p -values and z -statistics as outlined in Section 3.1.

The results reveal that in Scenario 1, the p -value is 0.2007 and the z -statistic is -1.2794 , indicating a decrease in model performance of more than one standard deviation from the baseline. In the more severe Scenario 2, the p -value drops to 0.0538 and the z -statistic reaches -1.9285 , corresponding to a decrease of nearly two standard deviations, while the even more severe Scenario 3 yields a p -value of 0.0173 and a z -statistic of -2.3805 . These findings demonstrate that more pronounced concept drift leads to stronger statistical evidence of model deterioration (indicated by lower p -values) and larger negative z -statistics. Moreover, they suggest that practitioners may benefit from adopting more conservative significance thresholds than the conventional level of 0.05 when monitoring models.

3.3 Practical Considerations and Pitfalls

In this section, we discuss practical considerations for implementing the proposed framework and summarize common pitfalls. We first list actionable setup recommendations, then a short checklist of basic pitfalls, and finally detail advanced pitfalls and their mitigations.

Practical considerations (setup and process):

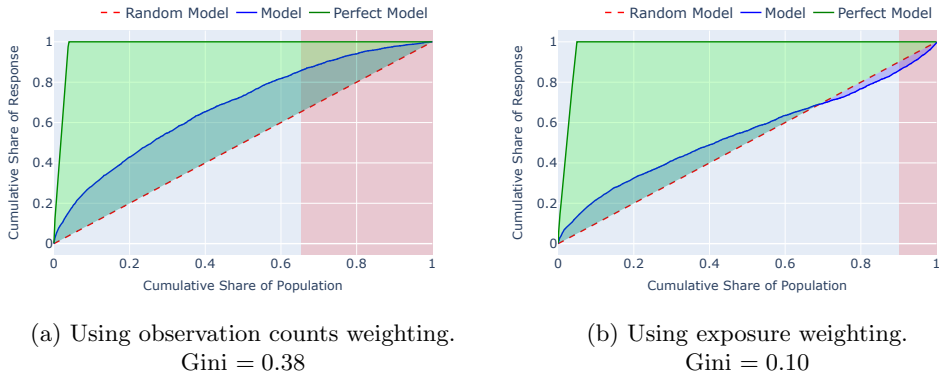
Significance level and monitoring frequency: Regarding the choice of significance level α , we deliberately choose not to recommend adopting a fixed level such as the commonly used $\alpha = 0.05$. The reason is that, in a model-monitoring context, the decision to replace a model typically involves a trade-off between performance considerations vs. stability and implementation costs, which is highly dependent on the specific business context. As mentioned above, the annual monitoring frequency is only an example; in reality, the monitoring cycle may vary depending on the model’s purpose as well as the business, implementation, and regulatory contexts.

Regarding the types of real concept drift: Depending on the detection of *real concept drift type* (see Section 2.1), one may use different holdout samples to estimate the mean and standard deviation of the Gini index based on the training period. For example, in the case of *sudden drift*, one might use a holdout sample consisting only of the most recent training year to estimate the mean and standard deviation of the Gini index. In cases of *gradual drift* or *incremental drift*, one might compute separate mean and standard deviation estimates for each training year’s holdout set, and conducting the hypothesis test separately for each year using its corresponding estimates. If *recurrent drift* due to seasonality is already known (e.g., weather-related monthly patterns), one should apply the above approach to datasets restricted to the relevant seasonal periods.

Exposure considerations in Gini calculation: Two related issues deserve attention. First, predictions must be adjusted for exposure (e.g., predicted counts = model prediction \times exposure) so that predictions and observations are on the same scale. Second, when constructing the CAP curve, decide whether the x-axis should accumulate observations (count weighting) or exposure (exposure weighting). In either case, due to Pitfall B (see below), it may be necessary to preaggregate the dataset at the policyholder level or at the level of unique covariate combinations (i.e., all covariates used in the model).

If the goal is to study the conditional distribution $F_{Y|\mathbf{X}}$ independently of $F_{\mathbf{X}}$, using observation counts as weights can be reasonable. If, on the other hand, one wants observations with larger exposure to contribute proportionally to the ranking and to the area under the CAP curve, consider exposure weighting.

Note that the choice of weighting can materially affect the Gini index. As an illustration, Figure 7 shows two CAP curves for the same dataset and model (discussed in Section 3.2) : one using observation counts weighting (left) and the other using exposure weighting (right).



The upper exposure decile contains:
 10.0% of the total exposure
 34.74% of the number of policies
 14.29% of the total response

Fig. 7: CAP curves using observation counts weighting (left) vs. exposure weighting (right). The upper exposure decile is marked light red. The dataset’s total number of observations is 64,978, total exposure is 35,967, and total response (claim count) is 2,645.

It is important to note that we used the same number of observations and adjusted the predictions for exposure in both cases, so the ordering of observations is identical. The only difference is the weighting of the x-axis in the CAP curve.

A substantial difference in the Gini index is clearly visible 0.38 versus 0.10 depending on the weighting choice. To illustrate why this occurs, we also report the composition of the upper exposure decile (i.e., the top 10% of the right x-axis). This decile corresponds to the 10% of total exposure with the lowest-ranked model predictions. Under exposure weighting, the upper decile contains 10.0% of the total exposure but represents 34.74% of all observations and 14.29% of the total response. This suggests that many observations with small exposure generated claims. Such a situation can occur, for example, when a claim represents a total loss of the vehicle, which typically leads to policy cancellation; and therefore smaller exposure as a result. I.e. the response influences the exposure. Because one often wishes to weigh those observations higher (despite their small exposure), one may reasonably prefer observation-count weighting over exposure weighting in such cases.

In summary, the choice of weighting can materially affect the Gini index and must be applied consistently.

Some pitfalls are often overlooked: while they matter less in model comparison settings, they can have a material impact in model-monitoring applications.

Basic pitfalls (quick checklist):

- Not using the holdout, but instead using the training data from the training period to estimate the parameters of the null distribution.
- Not considering exposure weights in the prediction.

- Not recognizing that exposure alone carries substantial explanatory power when interpreting the Gini index. (Consequently, a mean model that accounts for exposure can considerably outperform a random benchmark.)
- Not removing observations with zero exposure. (These will change the deviance and Gini measure depending on the implementation, due to their impact on the observation count.)
- Not ensuring model autocalibration during training (especially for ML-models like GBMs or NNs).
- Not considering the Gini’s limitations when reapplying a model: The Gini is rank-based; it does not detect systematic level shifts (e.g., uniformly over- or under-predicting frequency). So when reapplying the model, always complement the Gini comparison with a level check and calibration.
- Not using at least as many observations in the new data as were used for the bootstrap approach. This is crucial for ensuring the validity of the statistical tests, since the distribution of the test statistic is affected by sample size.

Advanced pitfalls (details and remedies):

Pitfall A: Implications of sorting ties in Gini calculation. Note that in the Definitions 4 and 5, we assume that $\hat{\mu}(\mathbf{X})$ has a continuous distribution. By contrast, the empirical Definitions 6 and 7 do not require this assumption. However, this can have material implications for the empirical Gini. In the empirical definition of the Gini index (see Definition 7), the sorting is based only on the predicted values $\hat{\mu}(\mathbf{X})$. Thus if the model is very small, the number of unique predicted values can be very small as well, and thus the sorting of the dataset effectively divides the data into just a few blocks. The CAP curve, and therefore the Gini, may then depend strongly on how observations within each tie are ordered. Because the empirical definition does not prescribe a tie-breaking rule, different implementations e.g. original order, random permutation, secondary sort by the observation, can yield noticeably different results.

In the following, we illustrate a scenario with limited data, where a small model with only a few covariates may be the only reasonable choice. For this purpose, we fitted a small GLM to the dataset discussed in Section 3.2. This GLM uses only a single categorical covariate with four unique values (we binned the numerical variable `DriveAge` into 4 buckets). To better visualize the impact, we took the above-mentioned dataset, and reduced it to only those observations with exposure $v_i = 1$. Since the model is so small and the exposure is uniformly equal to 1, sorting by the predictions partitions the data into exactly four blocks with tied predicted values within each block.

We visualize the CAP curves for different tie-breaking methods in the case of prediction ties in Figure 8. If observations with tied predicted values are sorted in random order (see (a) in Figure 8), this yields a plausible CAP curve and a Gini index of about 0.05, consistent with the limited discriminatory power of such a small model. When ties are ordered in the best possible way (see (b) in Figure 8), the Gini index increases to about 0.31. Finally, if ties are ordered in the worst possible way (see (c) in Figure 8), the Gini index becomes negative, around -0.21 . This would normally indicate that the model performs worse than random guessing, which is clearly not the case here, since there is no negative correlation between predictions and outcomes. Thus, the Gini index can vary substantially depending on how sortation is handled. For this reason, we do not recommend using best- or worst-case sortation, especially when the model produces only a small number of unique prediction values.

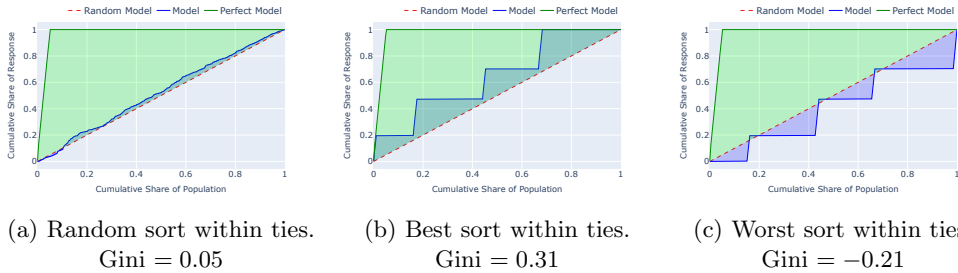


Fig. 8: CAP curves for a small GLM with different sorting methods for observations with tied predicted values.

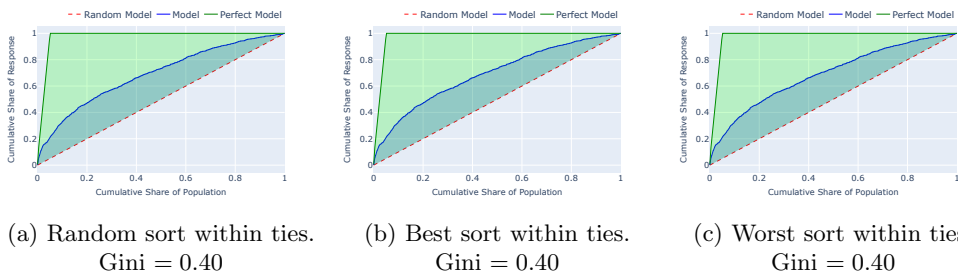


Fig. 9: CAP curves for a bigger GLM with different sorting methods for observations with tied predicted values.

This issue should arise only in small models with few covariates or in datasets with limited diversity. To illustrate, if we use the model described in Section 3.2 with higher discriminatory power on the same restricted dataset, we obtain a Gini index of about 0.40, independent of the sorting method used; see Figure 9.

Recommendation. As a practical solution, we suggest investing slightly more computation: compute the Gini index twice, once using the best-case and once using the worst-case ordering within ties, and use the average of these two values. For the small model, this yields a Gini index of about 0.05, identical to that from random tie-breaking but without dependence on a random seed. This approach does not adversely affect larger models with more unique predicted values.

Pitfall B: Implications of Time-split. The following aspect of the ETL pipeline for *model-monitoring* is often underestimated: In claim-frequency modeling, one typically works with datasets \mathcal{D} in which each row represents a specific time period for a policyholder. Even if a policy's covariates do not change, typical ETL pipelines will split these time periods for various reasons. This means that a policyholder's record is split into multiple rows representing shorter intervals (keeping the covariates unchanged, adjusting the exposure, and setting the target variable according to whether a claim occurred in the sub-interval), yielding a new dataset \mathcal{D}' . One reason for such time splitting is to simplify reporting: it is desirable to have at most one claim per row, so that the claim date and other information about the response

can be stored in that row (which would not easily be possible in traditional data structures if multiple claims occurred during the period and were aggregated).

This new dataset \mathcal{D}' has the same average claim frequency, the same total number of claims, and the same total exposure $\sum_{i=1}^n v_i$. Moreover, by inspecting the score equations, one can easily show that, e.g., in the Poisson GLM case, such a time-period split does not affect the model fit; i.e., the same GLM coefficients result regardless of whether the model was fitted to the dataset before time-period splitting \mathcal{D} or after time splitting to \mathcal{D}' . For this reason, ETL pipelines might incorporate many time splits so that the dataset can be reused for various purposes. While this may not affect the model selection process (such as in GLM modeling), it can have a large impact on the model monitoring process, because the Gini and deviance loss can change dramatically when time splits are applied, especially if those splits depend on the response.

To illustrate this issue, we provide an extreme example using the dataset and model described in Section 3.2. We applied a time-period split such that each claim is represented by exactly one row with an exposure of one day ($1/365$ of a year). In the case of rows with multiple claims, we created multiple one-day rows, each containing exactly one claim. The remaining exposure was assigned to an additional row with zero claims. We fitted the same model to this new dataset and obtained the same coefficients as before (up to numerical precision). However, the Gini index dropped from 0.38 to -0.99 , and the Poisson deviance loss increased from $24.941 \cdot 10^{-2}$ to $65.224 \cdot 10^{-2}$. The reason for this dramatic change can be clearly seen in the CAP curve shown in Figure 10.

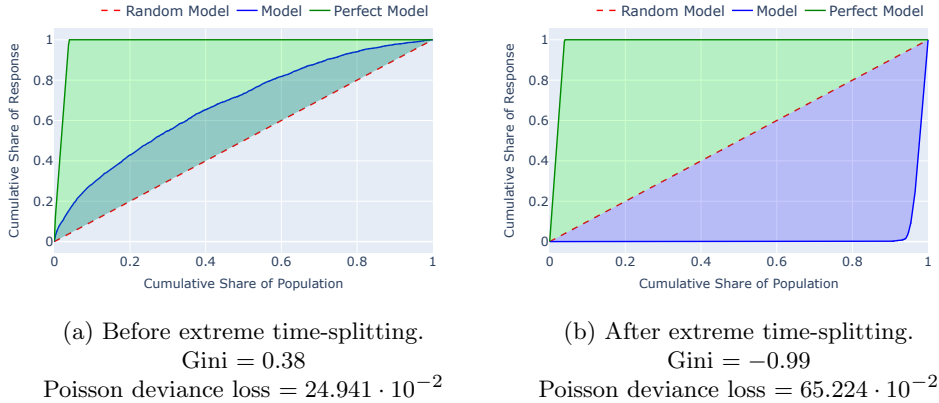


Fig. 10: CAP curves before extreme time-splitting (left) vs. after extreme time-splitting (right).

Due to the time-period split, the predictions are scaled by unrealistically small exposures; consequently, the ordering of observations changes substantially, leading to very different metrics. Since time-period splitting is routinely performed for various reasons in large ETL processes, this extreme example illustrates a potential pitfall: underestimating the effect of ETL changes that do not affect the model fit but do affect the model-monitoring process.

Recommendation. To avoid this pitfall, we suggest preaggregating the dataset before using it in a *model-monitoring* context, at least at the policyholder level or at the level of unique covariate combinations (i.e., all covariates used in the model). This will add a small amount

of computation to the ETL pipeline for the monitoring process but will also reduce model inference time because the dataset will be smaller.

4 Conclusion

This paper provides a systematic examination of concept drift in non-life insurance pricing and a statistically grounded monitoring framework. A comprehensive overview of the relevant literature on concept drift is provided and contextualized in the actuarial setting. We derive the asymptotic distribution of the Gini index to enable valid inference and hypothesis testing. Building on this, we propose a standardized monitoring procedure that signals when refitting is warranted and illustrate its practical use on a modified real-world portfolio in which we inject controlled levels of concept drift. We highlight implementation considerations and several pitfalls for model monitoring and model comparison.

Provided predictions are assessed under an auto-calibration perspective, the framework is model-agnostic and applies not just for GLMs but equally to modern machine-learning models such as tree ensembles and neural networks. In practice, the approach supports transparent and repeatable monitoring and governance, helping prioritize refitting efforts where they create the most value.

Methodologically, several extensions are promising and warrant exploration in future research. Different windowing designs and adaptive schemes could be investigated to improve responsiveness and robustness. Recurrent drift deserves special attention, particularly in long-term business. In addition, combining multiple concept drift detection methods with dimensionality-reduction diagnostics could improve attribution and reveal the drivers of drift. While the focus of our work is on drift detection, future work could benchmark drift-adaptation strategies for pricing, including windowing-based updates, ensemble methods, and continual learning to maintain performance while preserving valuable prior knowledge.

We hope these contributions encourage systematic, drift-aware monitoring and stimulate further research on adaptive actuarial modeling.

References

- Ackerman S, Raz O, Zalmanovici M, et al (2021) Automatically detecting data drift in machine learning classifiers. <https://doi.org/10.48550/arXiv.2111.05672>
- Bifet A, Gavaldà R (2007) Learning from Time-Changing Data with Adaptive Windowing. In: Proceedings of the 2007 SIAM International Conference on Data Mining (SDM). Proceedings, Society for Industrial and Applied Mathematics, p 443–448, <https://doi.org/10.1137/1.9781611972771.42>
- Billingsley P (1999) Convergence of Probability Measures. John Wiley & Sons, Ltd, <https://doi.org/10.1002/9780470316962>
- Brauer A (2024) Enhancing actuarial non-life pricing models via transformers. European Actuarial Journal 14(3):991–1012. <https://doi.org/10.1007/s13385-024-00388-2>
- Buitinck L, Louppe G, Blondel M, et al (2013) API design for machine learning software: experiences from the scikit-learn project. In: ECML PKDD Workshop:

Languages for Data Mining and Machine Learning, pp 108–122

- Charpentier A (2024) Insurance, biases, discrimination and fairness. Springer Actuarial, Springer, Cham, <https://doi.org/10.1007/978-3-031-49783-4>
- Davidson R (2009) Reliable inference for the Gini index. *Journal of Econometrics* 150(1):30–40. <https://doi.org/10.1016/j.jeconom.2008.11.004>
- Denuit M, Sznajder D, Trufin J (2019) Model selection based on Lorenz and concentration curves, Gini indices and convex order. *Insurance: Mathematics and Economics* 89:128–139. <https://doi.org/10.1016/j.insmatheco.2019.09.001>
- Denuit M, Charpentier A, Trufin J (2021) Autocalibration and Tweedie-dominance for insurance pricing with machine learning. *Insurance: Mathematics and Economics* 101:485–497. <https://doi.org/10.1016/j.insmatheco.2021.09.001>
- Denuit M, Huyghe J, Trufin J, et al (2024) Testing for auto-calibration with Lorenz and Concentration curves. *Insurance: Mathematics and Economics* 117:130–139. <https://doi.org/10.1016/j.insmatheco.2024.04.003>
- Dutang C, Charpentier A (2018) CASdatasets: Insurance datasets. URL <http://dutangc.free.fr/pub/RRepos/>, r package version 1.0–8
- Gama J, Medas P, Castillo G, et al (2004) Learning with Drift Detection. In: Bazzan ALC, Labidi S (eds) *Advances in Artificial Intelligence – SBIA 2004*. Springer, Berlin, Heidelberg, pp 286–295, https://doi.org/10.1007/978-3-540-28645-5_29
- Gama J, Žliobaitė I, Bifet A, et al (2014) A survey on concept drift adaptation. *ACM Comput Surv* 46(4):44:1–44:37. <https://doi.org/10.1145/2523813>
- Hinder F, Vaquet V, Hammer B (2024) One or two things we know about concept drift—a survey on monitoring in evolving environments. Part A: detecting concept drift. *Frontiers in Artificial Intelligence* 7. <https://doi.org/10.3389/frai.2024.1330257>, publisher: Frontiers
- Holvoet F, Antonio K, Henckaerts R (2025) Neural Networks for Insurance Pricing with Frequency and Severity Data: A Benchmark Study from Data Preprocessing to Technical Tariff. *North American Actuarial Journal* 29(3):519–562. <https://doi.org/10.1080/10920277.2025.2451860>
- Hu L, Lu Y, Feng Y (2025) Concept Drift Detection Based on Deep Neural Networks and Autoencoders. *Applied Sciences* 15(6):3056. <https://doi.org/10.3390/app15063056>, publisher: MDPI AG
- Krüger F, Ziegel JF (2021) Generic conditions for forecast dominance. *Journal of Business & Economic Statistics* 39(4):972–983. <https://doi.org/10.1080/07350015.2020.1741376>

- Lorentzen C, Mayer M (2020) Peeking into the Black Box: An Actuarial Case Study for Interpretable Machine Learning. <https://doi.org/10.2139/ssrn.3595944>
- Lu J, Liu A, Dong F, et al (2019) Learning under Concept Drift: A Review. *IEEE Transactions on Knowledge and Data Engineering* 31(12):2346–2363. <https://doi.org/10.1109/TKDE.2018.2876857>
- Mallick A, Hsieh K, Arzani B, et al (2022) Matchmaker: Data Drift Mitigation in Machine Learning for Large-Scale Systems. *Proceedings of Machine Learning and Systems* 4:77–94. URL https://proceedings.mlsys.org/paper_files/paper/2022/hash/069a002768bcb31509d4901961f23b3c-Abstract.html
- Nelder JA, Wedderburn RWM (1972) Generalized Linear Models. *Journal of the Royal Statistical Society Series A (General)* 135(3):370–384. <https://doi.org/10.2307/2344614>, publisher: [Royal Statistical Society, Wiley]
- Nishida K, Yamauchi K (2007) Detecting Concept Drift Using Statistical Testing. In: Corruble V, Takeda M, Suzuki E (eds) *Discovery Science*. Springer, Berlin, Heidelberg, pp 264–269, https://doi.org/10.1007/978-3-540-75488-6_27
- Noll A, Salzmann R, Wüthrich MV (2020) Case Study: French Motor Third-Party Liability Claims. <https://doi.org/10.2139/ssrn.3164764>
- Rabanser S, Günemann S, Lipton Z (2019) Failing loudly: An empirical study of methods for detecting dataset shift. *Advances in Neural Information Processing Systems* 32
- Richman R, Wüthrich MV (2023) LocalGLMnet: interpretable deep learning for tabular data. *Scandinavian Actuarial Journal* 2023(1):71–95. <https://doi.org/10.1080/03461238.2022.2081816>, publisher: Taylor & Francis
- Richman R, Scognamiglio S, Wüthrich MV (2025) The credibility transformer. *European Actuarial Journal* 15(2):345–379. <https://doi.org/10.1007/s13385-025-00413-y>
- Schlimmer JC, Granger RH (1986) Beyond incremental processing: tracking concept drift. In: *Proceedings of the Fifth AAAI National Conference on Artificial Intelligence*. AAAI Press, AAAI'86, p 502–507
- Van Der Vaart AW, Wellner JA (2023) *Weak Convergence and Empirical Processes: With Applications to Statistics*. Springer Series in Statistics, Springer International Publishing, Cham, <https://doi.org/10.1007/978-3-031-29040-4>
- Widmer G, Kubat M (1996) Learning in the presence of concept drift and hidden contexts. *Machine Learning* 23(1):69–101. <https://doi.org/10.1007/BF00116900>
- Wüthrich MV, Richman R, Avanzi B, et al (2025) AI Tools for Actuaries. <https://doi.org/10.2139/ssrn.5162304>

Wüthrich MV (2023) Model selection with Gini indices under auto-calibration. European Actuarial Journal 13(1):469–477. <https://doi.org/10.1007/s13385-022-00339-9>

Wüthrich MV (2025) Auto-calibration tests for discrete finite regression functions. European Actuarial Journal 15(1):335–341. <https://doi.org/10.1007/s13385-025-00410-1>

Wüthrich MV, Merz M (2023) Statistical foundations of actuarial learning and its applications. Springer Actuarial, Springer, Cham, Switzerland, <https://doi.org/10.1007/978-3-031-12409-9>

Appendix A Proof of Theorem 1

First we recall the theorem:

Theorem 2 (Asymptotic Normality of the Gini Index). *Assume $(Y_i, \mathbf{X}_i) \sim F \in \mathcal{F}$ i.i.d. and let $\hat{\mu}(\cdot)$ be an auto-calibrated estimator. Suppose $\mathbb{E}[Y] < \infty$ and $\mathbb{E}[\hat{\mu}(\mathbf{X})] < \infty$. Further assume that Y and $\hat{\mu}(\mathbf{X})$ have continuous distribution functions F_Y and $F_{\hat{\mu}(\mathbf{X})}$, respectively. Let the combined distribution function of $(Y, \hat{\mu}(\mathbf{X}))$ be denoted by $F_{Y, \hat{\mu}(\mathbf{X})}$ and the Gini index $G_{Y, \hat{\mu}(\mathbf{X})}$ be defined as in Definition 5.*

Then there is a functional T such that the Gini index can be written as $T(F_{Y, \hat{\mu}(\mathbf{X})}) = G_{Y, \hat{\mu}(\mathbf{X})}$ and the plug in estimator $\hat{G}_{Y, \hat{\mu}(\mathbf{X})} := T(\hat{F}_{Y, \hat{\mu}(\mathbf{X})})$ for the Gini index is asymptotically normal distributed. Specifically it holds for some $\sigma^2 > 0$, that

$$\sqrt{n}(\hat{G}_{Y, \hat{\mu}(\mathbf{X})} - G_{Y, \hat{\mu}(\mathbf{X})}) \xrightarrow{d} N(0, \sigma^2).$$

As mentioned in Section 2.2.3, the proof is carried out in the following three steps.

1. Represent the Gini index as a statistical functional T .
2. Show that T is Hadamard differentiable at $F_{Y, \hat{\mu}(\mathbf{X})}$.
3. Combine the empirical-process convergence $\sqrt{n}(\hat{F}_{Y, \hat{\mu}(\mathbf{X})} - F_{Y, \hat{\mu}(\mathbf{X})}) \rightsquigarrow \mathbb{G}_F$ with the functional Delta Method to obtain $\sqrt{n}(\hat{G}_{Y, \hat{\mu}(\mathbf{X})} - G_{Y, \hat{\mu}(\mathbf{X})}) \xrightarrow{d} N(0, \sigma^2)$.

We carry out these steps of the proof in the following subsections.

Proof of Theorem 1.

A.1 Gini Index as a Statistical Functional T

In the following, we adapt techniques from Davidson (2009), as well as insights from Proposition 4.1 in Wüthrich (2023). Recall that the Gini index is formally defined as:

$$G_{Y, \hat{\mu}(\mathbf{X})} := \frac{\int_0^1 \text{CAP}_{Y, \hat{\mu}(\mathbf{X})}(\alpha) d\alpha - \frac{1}{2}}{\int_0^1 \text{CAP}_{Y, Y}(\alpha) d\alpha - \frac{1}{2}}. \quad (\text{A1})$$

We start by reformulating the numerator.

$$\begin{aligned} \int_0^1 \text{CAP}_{Y, \hat{\mu}(\mathbf{X})}(\alpha) d\alpha - \frac{1}{2} &\stackrel{\text{Def. 4}}{=} \int_0^1 \frac{1}{\mathbb{E}[Y]} \mathbb{E} \left[Y \mathbb{1}_{\{\hat{\mu}(\mathbf{X}) > F_{\hat{\mu}(\mathbf{X})}^{-1}(1-\alpha)\}} \right] d\alpha - \frac{1}{2} \\ &\stackrel{(1)}{=} \int_0^1 \frac{1}{\mathbb{E}[Y]} \mathbb{E} \left[\mathbb{E} \left[Y \mathbb{1}_{\{\hat{\mu}(\mathbf{X}) > F_{\hat{\mu}(\mathbf{X})}^{-1}(1-\alpha)\}} \mid \mathbf{X} \right] \right] d\alpha - \frac{1}{2} \\ &\stackrel{(2)}{=} \int_0^1 \frac{1}{\mathbb{E}[Y]} \mathbb{E} \left[\mathbb{E}[Y \mid \mathbf{X}] \mathbb{1}_{\{\hat{\mu}(\mathbf{X}) > F_{\hat{\mu}(\mathbf{X})}^{-1}(1-\alpha)\}} \right] d\alpha - \frac{1}{2} \\ &\stackrel{(3)}{=} \int_0^1 \frac{1}{\mathbb{E}[Y]} \mathbb{E} \left[\hat{\mu}(\mathbf{X}) \mathbb{1}_{\{\hat{\mu}(\mathbf{X}) > F_{\hat{\mu}(\mathbf{X})}^{-1}(1-\alpha)\}} \right] d\alpha - \frac{1}{2} \\ &\stackrel{(4)}{=} \frac{1}{\mathbb{E}[Y]} \int_0^1 \int_0^\infty \mu \mathbb{1}_{\{\mu > F_{\hat{\mu}(\mathbf{X})}^{-1}(1-\alpha)\}} dF_{\hat{\mu}(\mathbf{X})}(\mu) d\alpha - \frac{1}{2} \\ &\stackrel{(5)}{=} \frac{1}{\mathbb{E}[Y]} \int_0^\infty \mu \int_{1-F_{\hat{\mu}(\mathbf{X})}(\mu)}^1 d\alpha dF_{\hat{\mu}(\mathbf{X})}(\mu) - \frac{1}{2} \\ &\stackrel{(6)}{=} \frac{1}{\mathbb{E}[Y]} \int_0^\infty \mu F_{\hat{\mu}(\mathbf{X})}(\mu) dF_{\hat{\mu}(\mathbf{X})}(\mu) - \frac{1}{2} \end{aligned}$$

The arguments rely on the tower property (1), basic properties of conditional expectations (2), the fact that the regression function is auto-calibrated (3), formulation of the expectation as a Riemann-Stieltjes integral (4), interchanging the order of integration and using that $F_{\hat{\mu}}^{-1}$ is non-decreasing and left-continuous (5) and finally evaluating the inner integral (6).

For the denominator, we can follow similar steps and obtain:

$$\int_0^1 \text{CAP}_{Y,Y}(\alpha) d\alpha - \frac{1}{2} = \frac{1}{\mathbb{E}[Y]} \int_0^\infty y F_Y(y) dF_Y(y) - \frac{1}{2}.$$

Using the expressions for the numerator and denominator derived above, we can now express the Gini index as their ratio and reformulate it as follows.

$$\begin{aligned} G_{Y,\hat{\mu}(\mathbf{X})} &= \frac{\frac{1}{\mathbb{E}[Y]} \int_0^\infty \mu F_{\hat{\mu}(\mathbf{X})}(\mu) dF_{\hat{\mu}(\mathbf{X})}(\mu) - \frac{1}{2}}{\frac{1}{\mathbb{E}[Y]} \int_0^\infty y F_Y(y) dF_Y(y) - \frac{1}{2}} \\ &\stackrel{(1)}{=} \frac{\int_0^\infty 2\mu F_{\hat{\mu}(\mathbf{X})}(\mu) dF_{\hat{\mu}(\mathbf{X})}(\mu) - \mathbb{E}[Y]}{\int_0^\infty 2y F_Y(y) dF_Y(y) - \mathbb{E}[Y]} \\ &\stackrel{(2)}{=} \frac{\int_0^\infty 2\mu F_{\hat{\mu}(\mathbf{X})}(\mu) dF_{\hat{\mu}(\mathbf{X})}(\mu) - \mathbb{E}[\hat{\mu}(\mathbf{X})]}{\int_0^\infty 2y F_Y(y) dF_Y(y) - \mathbb{E}[Y]} \\ &\stackrel{(3)}{=} \frac{\int_0^\infty 2\mu F_{\hat{\mu}(\mathbf{X})}(\mu) dF_{\hat{\mu}(\mathbf{X})}(\mu) - \int_0^\infty \mu dF_{\hat{\mu}(\mathbf{X})}(\mu)}{\int_0^\infty 2y F_Y(y) dF_Y(y) - \int_0^\infty y dF_Y(y)} \\ &\stackrel{(4)}{=} \frac{\int_0^\infty (2\mu F_{\hat{\mu}(\mathbf{X})}(\mu) - \mu) dF_{\hat{\mu}(\mathbf{X})}(\mu)}{\int_0^\infty (2y F_Y(y) - y) dF_Y(y)} \\ &\stackrel{(5)}{=} \frac{\int_{[0,\infty)^2} \left[2\mu \left(\int_{[0,\infty)^2} \mathbb{1}_{\{t \in [0,\mu]\}} dF_{(\hat{\mu}(\mathbf{X}),Y)}(t,s) \right) - \mu \right] dF_{(\hat{\mu}(\mathbf{X}),Y)}(\mu,y)}{\int_{[0,\infty)^2} \left[2y \left(\int_{[0,\infty)^2} \mathbb{1}_{\{s \in [0,y]\}} dF_{(\hat{\mu}(\mathbf{X}),Y)}(t,s) \right) - y \right] dF_{(\hat{\mu}(\mathbf{X}),Y)}(\mu,y)} \\ &= \frac{T_1(F_{(\hat{\mu}(\mathbf{X}),Y)})}{T_2(F_{(\hat{\mu}(\mathbf{X}),Y)})} =: T(F_{(\hat{\mu}(\mathbf{X}),Y)}). \end{aligned}$$

Here we multiply the numerator and denominator by $2\mathbb{E}[Y]$ in (1), use the fact that auto-calibration implies unbiasedness in (2), rewrite the expectations as Riemann-Stieltjes integrals in (3), combine the integrands in (4), and finally express the distribution functions in terms of the joint distribution in (5). This completes the first step of the proof, as we express the Gini index as a functional T of the joint distribution function $F_{(\hat{\mu}(\mathbf{X}),Y)}$.

A.2 Hadamard-Differentiability of the Functional T

Before we start, we refer to Section 3.10 in [Van Der Vaart and Wellner \(2023\)](#) regarding Hadamard-differentiability. Let \mathfrak{F} be the normed linear spaces of all linear combinations of CDF's of random variables with finite expectation.

Note that the functional T can be expressed as the ratio of two functionals T_1 and T_2 , where T_1 is the numerator and T_2 is the denominator of T .

We examine the denominator T_2 and represent it as a functional $\tilde{T}_2(\cdot)$ of F_Y that is

Hadamard-differentiable at F_Y . The same arguments apply to the numerator T_1 .

$$\begin{aligned} T_2(F_{(\hat{\mu}(\mathbf{X}), Y)}) &= \int_{[0, \infty)^2} \left[2y \left(\int_{[0, \infty)^2} \mathbb{1}_{\{s \in [0, y]\}} dF_{(\hat{\mu}(\mathbf{X}), Y)}(t, s) \right) - y \right] dF_{(\hat{\mu}(\mathbf{X}), Y)}(\mu, y) \\ &= \int_0^\infty 2y F_Y(y) - y dF_Y(y) =: \tilde{T}_2(F_Y), \end{aligned}$$

We can split $\tilde{T}_2(F_Y)$ into two functionals $\tilde{T}_{2,a}$ and $\tilde{T}_{2,b}$ such that $\tilde{T}_2(F_Y) = \tilde{T}_{2,a}(F_Y) - \tilde{T}_{2,b}(F_Y)$ with

$$\begin{aligned} \tilde{T}_{2,a}(F_Y) &:= \int_0^\infty 2y F_Y(y) dF_Y(y), \\ \tilde{T}_{2,b}(F_Y) &:= \int_0^\infty y dF_Y(y). \end{aligned}$$

By showing that both $\tilde{T}_{2,a}$ and $\tilde{T}_{2,b}$ are Hadamard-differentiable at F_Y , we show that \tilde{T}_2 is Hadamard-differentiable at F_Y by the Chain Rule (Lemma 3.10.9 in [Van Der Vaart and Wellner \(2023\)](#)).

Recall that a functional $T : \mathfrak{F} \rightarrow \mathbb{R}$ is called Hadamard-differentiable at F_Y if there is a continuous linear map $T'_{F_Y} : \mathfrak{F} \rightarrow \mathbb{R}$ such that

$$\sup_{H \in K, F_Y + tH \in \mathfrak{F}} \left\| \frac{T(F_Y + tH) - T(F_Y)}{t} - T'(H) \right\| \rightarrow 0, \text{ as } t \rightarrow 0,$$

for every compact $K \subset \mathfrak{F}$ (see Equation (3.10.1) in [Van Der Vaart and Wellner \(2023\)](#)).

For $\tilde{T}_{2,b}$ we have:

$$\begin{aligned} \frac{\tilde{T}_{2,b}(F_Y + tH) - \tilde{T}_{2,b}(F_Y)}{t} &= \frac{1}{t} \left(\int_0^\infty y d(F_Y(y) + tH(y)) - \int_0^\infty y dF_Y(y) \right) \\ &= \int_0^\infty y dH(y). \end{aligned}$$

Setting $\tilde{T}'_{2,b}(H) := \int_0^\infty y dH(y)$, it is left to show that $\tilde{T}'_{2,b}$ is a continuous linear map. Linearity follows directly from the linearity of the Riemann-Stieltjes integral. To show continuity, we need to show that for a sequence $H_n \rightarrow H$ in \mathfrak{F} it holds that $\tilde{T}'_{2,b}(H_n) \rightarrow \tilde{T}'_{2,b}(H)$.

$$\begin{aligned} \lim_{n \rightarrow \infty} \left| \tilde{T}'_{2,b}(H_n) - \tilde{T}'_{2,b}(H) \right| &= \lim_{n \rightarrow \infty} \left| \int_0^\infty y dH_n(y) - \int_0^\infty y dH(y) \right| \\ &\stackrel{(1)}{=} \lim_{n \rightarrow \infty} \left| \int_0^\infty y d(H_n(y) - H(y)) \right| \\ &\stackrel{(2)}{=} \lim_{n \rightarrow \infty} \left| \int_0^m y d(H_n(y) - H(y)) + \int_m^\infty y d(H_n(y) - H(y)) \right| \\ &\stackrel{(3)}{=} \lim_{n \rightarrow \infty} \left| [y(H_n(y) - H(y))]_0^m - \int_0^m H_n(y) - H(y) dy + \int_m^\infty y d(H_n(y) - H(y)) \right| \\ &\stackrel{(4)}{\leq} \lim_{n \rightarrow \infty} |m(H_n(m) - H(m))| + \lim_{n \rightarrow \infty} \left| \int_0^m H_n(y) - H(y) dy \right| + \lim_{n \rightarrow \infty} \left| \int_m^\infty y d(H_n(y) - H(y)) \right| \\ &\stackrel{(5)}{=} \lim_{n \rightarrow \infty} \left| \int_m^\infty y d(H_n(y) - H(y)) \right| \\ &\stackrel{(6)}{\leq} \lim_{n \rightarrow \infty} \left| \int_m^\infty y dH_n(y) \right| + \lim_{n \rightarrow \infty} \left| \int_m^\infty y dH(y) \right|, \end{aligned}$$

where we use the linearity of the integral in (1), split the integral at some point m (2), use integration by parts in (3), and apply the triangle inequality in (4). The first two terms vanish because the supremum of $|H_n(y) - H(y)|$ converges to zero for $H_n \rightarrow H$ and (6) uses again the triangle inequality. Finally note that H_n and H are in \mathfrak{F} , so they can be represented as linear combinations of CDF's with finite expectation. Therefore,

$$\int_m^\infty y dH(y) = \int_m^\infty y d\left(\sum_{i=1}^{\hat{k}} \hat{\lambda}_i \hat{H}_i(y)\right) = \sum_{i=1}^{\hat{k}} \hat{\lambda}_i \int_m^\infty y d\hat{H}_i(y). \quad (\text{A2})$$

Furthermore, with the same argument as in the proof of Theorem 3.5 in Billingsley (1999), we can state for a given ϵ there is an m such that $\int_m^\infty y d\hat{H}_i(y) < \epsilon$ for all $i = 1, \dots, \hat{k}$. And therefore there is a constant C s.t. $|\int_m^\infty y dH(y)| < \epsilon C$. Since we can apply the same argument to the integral with respect to H_n , we can conclude that

$$\lim_{n \rightarrow \infty} \left| \tilde{T}'_{2,b}(H_n) - \tilde{T}'_{2,b}(H) \right| \leq \epsilon \tilde{C}.$$

But since ϵ is arbitrary, we show the continuity of $\tilde{T}'_{2,b}$.

For $\tilde{T}'_{2,a}$ we have:

$$\begin{aligned} \frac{\tilde{T}'_{2,a}(F_Y + tH) - \tilde{T}'_{2,a}(F_Y)}{t} &= \frac{1}{t} \left(\int_0^\infty 2y(F_Y(y) + tH(y)) d(F_Y(y) + tH(y)) - \int_0^\infty 2yF_Y(y) dF_Y(y) \right) \\ &= \int_0^\infty 2yH(y) dF_Y(y) + \int_0^\infty 2yF_Y(y) dH(y) + t \int_0^\infty 2yH(y) dH(y). \end{aligned}$$

Setting $\tilde{T}'_{2,a}(H) := \int_0^\infty 2yH(y) dF_Y(y) + \int_0^\infty 2yF_Y(y) dH(y)$, we obtain

$$\begin{aligned} \sup_{H \in K, F_Y + tH \in \mathfrak{F}} \left| \frac{\tilde{T}'_{2,a}(F_Y + tH) - \tilde{T}'_{2,a}(F_Y)}{t} - \tilde{T}'_{2,a}(H) \right| &= \sup_{H \in K, F_Y + tH \in \mathfrak{F}} \left| t \int_0^\infty 2yH(y) dH(y) \right| \\ &\stackrel{(1)}{\leq} 2|t| C_1 \sup_{H \in K} \left| \int_0^\infty y dH(y) \right| \\ &\stackrel{(2)}{\leq} 2|t| C_1 C_2 \rightarrow 0, \text{ as } t \rightarrow 0, \end{aligned}$$

where (1) uses the fact that H is a linear combination of CDF's and therefore bounded by some constant C_1 , and (2) uses that H is a linear combination of CDF's with finite expectation and therefore $\int_0^\infty y dH(y)$ is bounded by some constant C_2 .

So it is left to show that $\tilde{T}'_{2,a}$ is a continuous linear map. Linearity follows again directly from the linearity of the Riemann-Stieltjes integral. To show continuity, we need to show

that for a sequence $H_n \rightarrow H$ in \mathfrak{F} it holds that $\tilde{T}'_{2,a}(H_n) \rightarrow \tilde{T}'_{2,a}(H)$.

$$\begin{aligned}
& \lim_{n \rightarrow \infty} \left| \tilde{T}'_{2,a}(H_n) - \tilde{T}'_{2,a}(H) \right| \\
&= \lim_{n \rightarrow \infty} \left| \int_0^\infty 2yH_n(y) dF_Y(y) + \int_0^\infty 2yF_Y(y) dH_n(y) \right. \\
&\quad \left. - \int_0^\infty 2yH(y) dF_Y(y) - \int_0^\infty 2yF_Y(y) dH(y) \right| \\
&\leq \lim_{n \rightarrow \infty} \left| \int_0^\infty 2y(H_n(y) - H(y)) dF_Y(y) \right| + \lim_{n \rightarrow \infty} \left| \int_0^\infty 2yF_Y(y) d(H_n(y) - H(y)) \right| \\
&\stackrel{(1)}{=} \lim_{n \rightarrow \infty} \left| \int_0^\infty 2y(H_n(y) - H(y)) dF_Y(y) \right| \\
&\stackrel{(2)}{\leq} \lim_{n \rightarrow \infty} \sup_y |H_n(y) - H(y)| \cdot \left| \int_0^\infty 2y dF_Y(y) \right| = 0,
\end{aligned}$$

where (1) uses that F_Y is bounded and the same arguments as in $T'_{2,b}$ to show that the second term vanishes, and (2) uses that F_Y is a CDF with finite expectation and therefore $\int_0^\infty 2y dF_Y(y)$ is finite.

We have shown that both $\tilde{T}_{2,a}$ and $\tilde{T}_{2,b}$ are Hadamard-differentiable at F_Y , and therefore \tilde{T}_2 is Hadamard-differentiable at F_Y . By applying the same arguments to T_1 , we conclude that T_1 is Hadamard-differentiable at $F_{(\hat{\mu}(\mathbf{X}), Y)}$. Finally, by the Chain Rule (Lemma 3.10.9 in [Van Der Vaart and Wellner \(2023\)](#)), we conclude that $T = \frac{T_1}{T_2}$ is Hadamard-differentiable at $F_{(\hat{\mu}(\mathbf{X}), Y)}$. Note $T_2(F_{(\hat{\mu}(\mathbf{X}), Y)}) > 0$, because $\int_0^1 \text{CAP}_{Y,Y}(\alpha) d\alpha - \frac{1}{2} > 0$ and $\mathbb{E}[Y]$ is finite.

We conclude that the Gini index $G_{Y, \hat{\mu}(\mathbf{X})}$ can be represented as a functional T that is Hadamard-differentiable at $F_{(\hat{\mu}(\mathbf{X}), Y)}$.

A.3 Application of the Functional Delta Method

Using Example 2.1.3 and 2.8.2 Donsker Theorem from [Van Der Vaart and Wellner \(2023\)](#) for the empirical distribution function with $(Y_i, \hat{\mu}(\mathbf{X}_i))$ i.i.d., it holds that

$$\sqrt{n} \left(\hat{F}_{Y, \hat{\mu}(\mathbf{X})} - F_{Y, \hat{\mu}(\mathbf{X})} \right) \xrightarrow{d} \mathbb{G},$$

where \mathbb{G} is a tight, Borel measurable Gaussian process with mean zero, called *Brownian bridge*.

Finally, we apply the delta method (Theorem 3.10.4 [Van Der Vaart and Wellner \(2023\)](#)) to conclude:

$$\sqrt{n} \left(\hat{G}_{Y, \hat{\mu}(\mathbf{X})} - G_{Y, \hat{\mu}(\mathbf{X})} \right) \xrightarrow{d} T'(\mathbb{G}),$$

where $T'(F_{Y, \hat{\mu}(\mathbf{X})})$ is the Hadamard derivative of the Gini index at $F_{Y, \hat{\mu}(\mathbf{X})}$, which is (per definition of the Hadamard derivative) a continuous and linear functional. By applying Lemma 3.10.8 in [Van Der Vaart and Wellner \(2023\)](#) we observe that $T'(\mathbb{G})$ is again normally distributed, since it is a linear functional of the Gaussian process \mathbb{G} . Thus we finally conclude that the Gini index is asymptotically normal. \square